Optical Feasibility Study on a 4-layer Cover-Incident Near-Field Recording System

J.M.A. van den Eerenbeemd*, F. Zijp, S. Stallinga

Philips Research Laboratories, High Tech Campus 34, 5656 AE Eindhoven, the Netherlands

ABSTRACT

We present a study on the feasibility of extending our current experimental cover-incident near-field recording system to a 4-layer system promising 500 GB storage capacity on a single sided 12 cm disc. We calculated the electromagnetic field inside a 4-layer disc of which the design was optimized to have a minimum in the irradiance near recording layers other than the one that the light is focused on. Furthermore an objective lens and compensation device were designed to accommodate writing and reading from all four layers.

Keywords: near-field optics, optical recording, vector diffraction theory, lens design

1. INTRODUCTION

Initial work on near-field (NF) recording work was focused on first surface systems[1,2]. In this case the data sits on the top surface of the disc and is very vulnerable for, e.g. small scratches. In all optical disc standards so far a cover-layer protects the data. To obtain a similar protection for NF recording media, we proposed a thin cover-layer of typically 3 μm thickness[1].

In separate contributions to these proceedings[3,4] we show experimental results with such a system and we present how cover-incident NF systems can open a roadmap towards a 500 GB storage capacity on a single sided disc by using four data layers, a Numerical Aperture (NA) of 1.6 and advanced signal processing[5]. For the design of such a system, the structure of the electromagnetic field and the aberrations inside the stack are important. In this paper we present calculation results on an example of a stack design that was optimized using these calculations. Also an objective lens design with an active compensation for jumping between the layers is presented.

In the cover-incident NF system the NA exceeds unity and therefore coupling of evanescent waves through a small air gap has to be taken into account in evaluating such a system. The evanescent coupling takes place between the exit surface of the Solid Immersion Lens (SIL) and the top of the cover, which is many wavelengths away from the spot at the data layer. This kind of system is very hard to be dealt with using e.g. finite element, finite difference time domain (FDTD) or Green's tensor methods because the calculation volume is typically 10 μm^3 or 150 λ^3 for a single layer system. This is 2 orders of magnitude larger than what currently can be conveniently handled using these methods. Other methods like geometrical, scalar diffractive or full vector diffraction inside a homogeneous medium[7] oversimplify the problem as the effects of evanescent coupling and the interference between multiple reflections inside the disc are not taken into account.

However, for calculating the spot inside a stack of layers without grooves or other topographical features the diffraction integral can be solved while taking evanescent coupling, multiple reflections, polarization and interference effects into account. We implemented the theory presented in Ref. 8 complemented with an exact wave-front aberration analysis[9] for arbitrary high NA and used it to evaluate the field inside the recording layers and calculate the spot shape for a 4-layer cover-incident NF recording system with an NA=1.6.

In the next section first some system choices are presented after which a system is proposed that will be used in the remainder of the paper. In section 3 the theory for calculating the electric fields inside the multi-layer stack will be summarized together with a calculation result. The lens design and an active compensation device will be shown in section 4. Section 5 will end this paper with a summary and conclusions.

* Jack.van.den.Eerenbeemd@philips.com; phone +31-40-2747795; fax +31-40-2746321

Optical Data Storage 2006, edited by Ryuichi Katayama, Tuviah E. Schlesinger
Proc. of SPIE Vol. 6282, 62820Q, (2006) · 0277-786X/06/$15 · doi: 10.1117/12.685216

2. SYSTEM CHOICES AND DESCRIPTION

In a multi-layer recording system data layers are separated by spacer layers. These data layers need to absorb and reflect light, but must also be (semi-) transparent because also the deeper layers need to be read. The separation between the data layers is in the order of several wavelengths and therefore smaller than the coherence length of the laser light. This layer stack acts as a Fabry-Perot type of interferometer and will give rise to strong interference effects due to multiple reflections. To simulate the interference from multiple reflections in a four-layer NF recording system, silver layers were used (n=0.174+i1.95) in a design example. The silver thickness of each data layer was tuned to obtain an integrated reflectivity of 4% in the pupil. The air gap was chosen to be 30 nm, which ensures that the evanescent part of the beam crosses the gap. The illumination of the entrance pupil is circularly polarized. The resulting stack as used for the calculations in this paper is shown in Fig. 1, with n_{cover}=n_{spacer}=1.7 and n_{SIL}=1.918.

The choices for the refractive indices mentioned in the former paragraph are based on reducing the spherical aberration in the system while achieving as high *NA* as possible. Choosing a difference as small as possible between the refractive indices n of the SIL and the cover-layer, see Fig. 2, reduces the amount of spherical aberration induced by the cover-layer. But, reducing the refractive index of the SIL, will increase the required numerical aperture NA_0 of the objective lens without the SIL in order to obtain our target effective numerical aperture of $NA_{eff} = n_{SIL}\, NA_0 = 1.6$ with a SIL. The maximum refractive index of the cover-layer material is limited by available materials that can be spin-coated onto a disc yielding several micrometers thick spacer and cover-layers. Using N-LaSF31 glass with n_{SIL}=1.918 for the SIL, requires an objective lens design with a NA_0=0.83 which is somewhat smaller than that of a Blu-ray Disc system. A suitable spin-coatable cover material with a refractive index of 1.7 is currently under development.

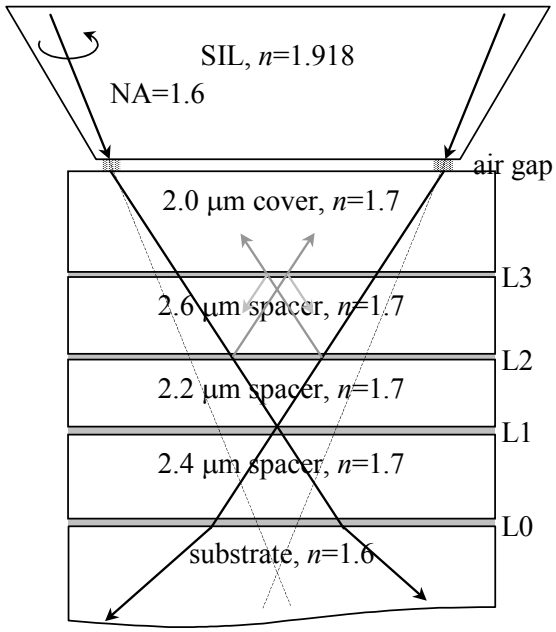

Fig. 1. Layout of the model used to simulate the 4-layer NF system. The L0-L3 layers are thin silver layers of respectively 6, 6, 5 and 5 nm thick. The air gap has a thickness equal to 30 nm. The incident beam is circularly polarized with *NA*=1.6 and a vacuum wavelength of λ_0=405 nm. The solid black lines indicate a 'ray'-path focusing at the L1 layer. The crossing of the dashed lines locates the focus in case the entire space consists of one single material. This is called the undisturbed focus position. The solid gray lines represent some reflected 'ray'-paths giving rise to a ghost focus near the L3 recording layer.

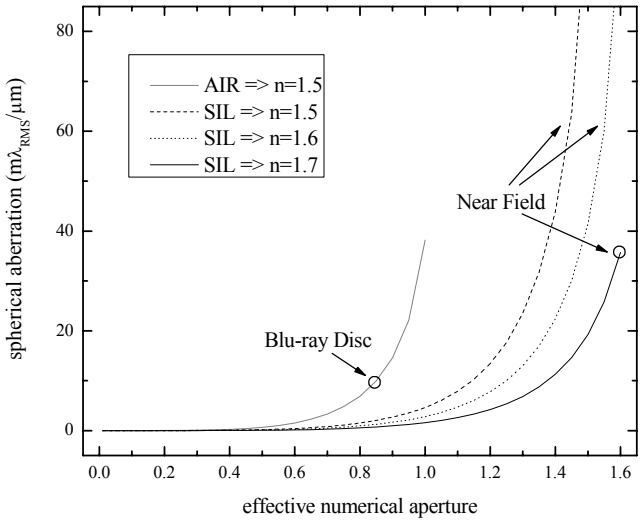

Fig. 2. Spherical aberration per unit thickness of cover layer as function of the effective numerical aperture for different cover materials in combination with a SIL compared to the conventional far-field optical recording case with n=1.5 for the cover-layer (BD) or substrate (CD/DVD). The curves are calculated using the expressions in the appendix.

The maximum of the sum of the thicknesses of the spacer layers is determined by the amount of spherical aberration that can be corrected by the light path. For a four-layer Blu-ray Disc the sum of the spacer layer thickness is 30 ~ 45 μm which means that, with 10 $m\lambda_{rms}/\mu m$ (see Fig. 2) spherical aberration, a total of 300 ~ 450 $m\lambda_{rms}$ must be corrected when jumping between layers. The spherical aberration per unit thickness of the cover and spacer-layers for our NA_{eff}=1.6 system amounts to 35.7 $m\lambda_{rms}/\mu m$ (again see Fig. 2). For the design in Fig. 1, the sum of the spacer layer thicknesses is 7.2 μm, which translates to an amount of spherical aberration equal to 275 $m\lambda_{rms}$, a value lower than for the BD-system. The minimum thickness of the individual spacer layers is determined by coherent cross-talk between the data-layers, here we use the estimate of 1.3 μm from earlier work as the lower limit[1].

3. SPOT CALCULATIONS

3.1. Theory

Our calculations of the electric field inside a multi-layer disc structure are based on a known formalism[8] for numerical evaluation of a full-vector diffraction integral inside a multi-layer structure. The formalism correctly accounts for all effects due to propagating and evanescent waves, polarization effects and multiple reflections inside a multi-layer structure of flat layers. No disc structures such as pits, grooves or recorded marks were included in our calculations. An extensive description of the theory used is beyond the scope of this paper and can be found in literature[8]. Instead, we briefly summarize the basics, starting with the well-known diffraction integral[7] for the field structure $\tilde{\boldsymbol{E}} = (\tilde{E}_x, \tilde{E}_y, \tilde{E}_z)$ at Cartesian coordinates (*x, y, z*) in a homogenous focal region:

$$\tilde{\boldsymbol{E}}(x,y,z) = -\frac{i}{2\pi}\iint_{\Omega} \frac{\boldsymbol{U}(k_x,k_y)}{k_z} e^{i(k_x x + k_y y + k_z z)} dk_x dk_y \tag{3.1}$$

where $\boldsymbol{U}(k_x,k_y)$ is the amplitude of a plane-wave with propagation vector $\boldsymbol{k} = (k_x,k_y,k_z)$ and the integration is over the exit pupil Ω with $k_x^2 + k_y^2 \le NA^2 k^2$ and $k = |\boldsymbol{k}| = 2\pi n/\lambda_0$. For an aplanatic lens of focal length *f* that obeys Abbe's sine condition, $\boldsymbol{U}(k_x,k_y)$ is found by first projecting the field $\boldsymbol{E}(k_x,k_y)$ in the entrance pupil on the exit pupil and a multiplication with *f*. To conserve energy in the transition from the entrance to the exit pupil the length of the field vector is scaled. The lens action rotates the field vector around an azimuthal axis in the exit pupil in accordance with the new direction of the plane wave. We can take advantage of the rotation symmetry of the lens by introducing cylindrical coordinates (r,φ,z) in the exit pupil and focal region such that $\boldsymbol{k} = (k_r,k_\varphi,k_z)$ with $k_z = (k^2 - k_r^2)^{1/2}$. Inside a multi-layer structure that consists of *N* media we have forward and backward propagating or evanescent plane waves of certain amplitude and phase. These are determined by the polarization state of the plane wave, the angle of incidence on the multi-layer structure and the Fresnel reflection and transmission coefficients for each layer transition and the optical thickness of each layer. We can now rewrite the diffraction integral in cylindrical coordinates and include both forward and backward propagating or evanescent plane waves:

$$\tilde{\boldsymbol{E}}(r,\varphi,z) = -\frac{if}{2\pi}\int_0^{2\pi}\int_0^{NAk_0} \frac{e^{ik_r r\cos(k_\varphi-\varphi)}}{\sqrt{k_{z1}k_1}} \left[\boldsymbol{M}_i^{+} e^{ik_{zi}z} + \boldsymbol{M}_i^{-} e^{-ik_{zi}z}\right] \boldsymbol{E}(k_r,k_\varphi) k_r dk_r dk_\varphi \tag{3.2}$$

with $k_{zi} = (k_i^2 - k_r^2)^{1/2}$ and in which the matrices $\boldsymbol{M}_i^{\pm}$ describe the vector rotation in the transition from entrance to exit pupil, the vector rotation inside layer *i* of the multi-layer structure and field amplitude factors for the TE and TM polarization states. The subscript $i = 1,2,3\ldots N$ refers to the properties of layer *i* with the exit pupil in layer $i = 1$ and the + and - superscripts indicate the forward and backward propagating or evanescent waves respectively. A derivation of matrices $\boldsymbol{M}_i^{\pm}$ is given in Ref. 8. A numerical evaluation of the above integral was implemented in computer code together with a code that calculates the TE and TM field amplitudes for the forward and backward propagating and evanescent plane waves inside each layer. The above integral is numerically evaluated by integrating the complex amplitude distribution in the *k*-space Ω. From the phase profile in Ω one can derive the required wave-front aberration correction to the field in the entrance pupil $\boldsymbol{E}(k_r,k_\varphi)$.

There are three contributions to the wave-front aberrations at the any of the four focus positions. By far the largest contribution can be explained using geometrical optics and is similar to the spherical aberration that is caused by focusing through a substrate in conventional optical recording systems. The two smaller contributions are due to the evanescent coupling in the air gap and the interference of forward and backward propagating waves in the four-layer disc structure. The amount and shape of the wave front aberration that is due to geometrical optics does not depend on the chosen state of polarization in the entrance pupil. The amount and shape of the wave front aberration that is due to the evanescent coupling and interference effects, however, does depend on the chosen state of polarization e.g. when linearly polarized light is used a significant amount of astigmatism is induced.[1] Our analysis shows that such non-rotationally symmetric polarization induced aberrations vanish when using circularly polarized light. The wave-front aberrations due to geometrical optics are of relatively low order and are easily corrected in the aspherical objective lens design. This correction is not perfect as evanescent coupling and multiple reflections inside the multi-layer stack cause small amounts of (high order) spherical aberration.

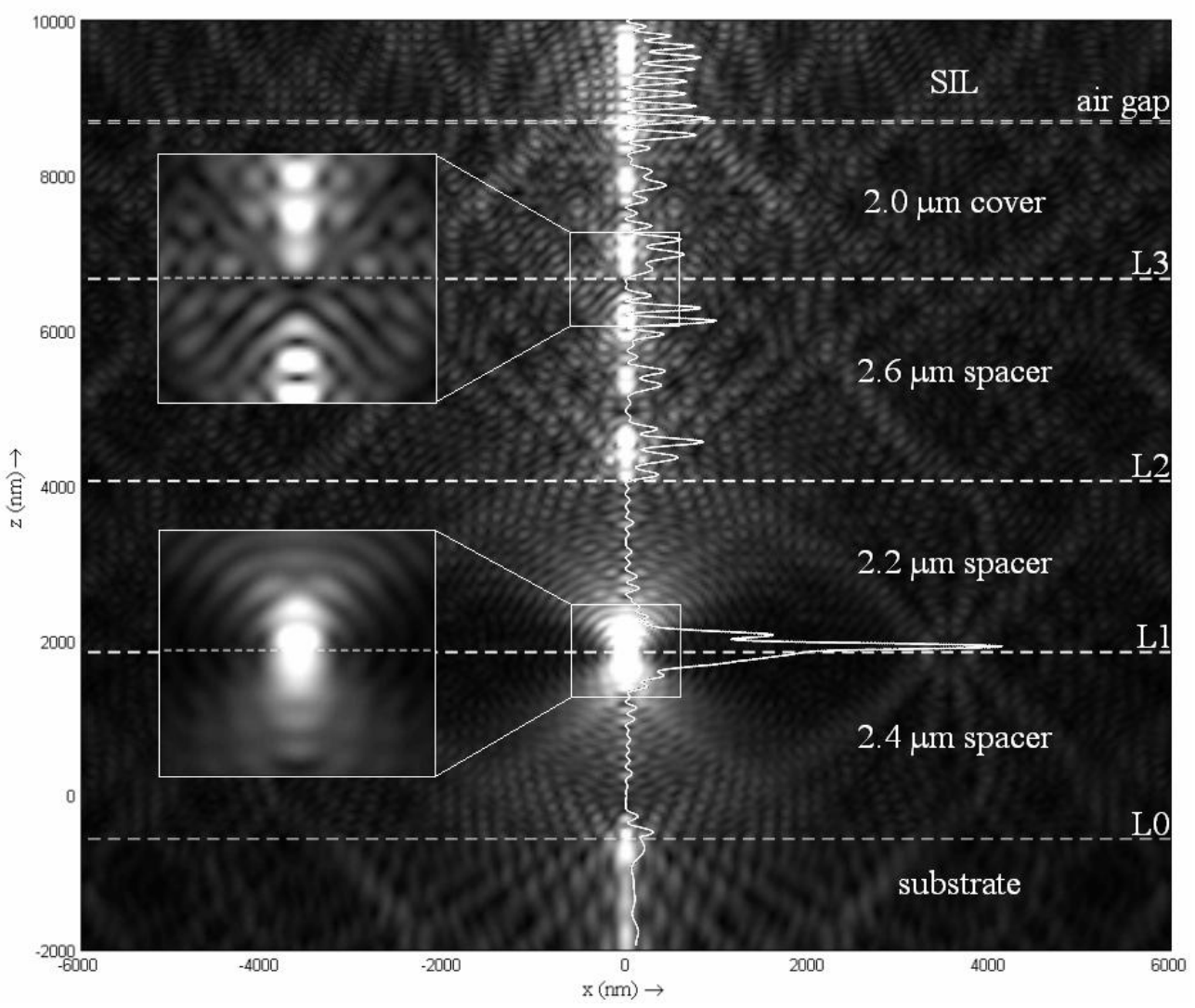

Fig. 3. Linear grayscale plot of the absolute value of the electric field |E| as function of the *x*- and *z*- coordinates. The light is focused at the L1 layer. In the large plot the values are clipped at 20% of the maximum value to make the structure of the field visible in the low irradiance regions. In the upper/lower inset the values are clipped at 30%/60%. The white line shows the (not clipped) irradiance value $I \propto |E|^2$ on the optical axis as function of the z-coordinate. The zero irradiance axis coincides with the optical axis at $x=0$. The peak value near the focus at the L1 layer is a factor 12 larger than the maximum value near any other layer.

The wave-front aberrations due to geometrical optics at the focus position on the chosen data layer (L1 in the figure) are minimized by correctly positioning the undisturbed focus (see Fig. 1). In the appendix we derive exact expressions for arbitrarily high NA for this focal shift and the Zernike coefficients associated with the wave-front aberration caused by focusing through a single interface between two transparent media. The undisturbed focus positions are calculated using the approximation of a single interface between SIL and the disc, in the absence of air gap and data layers. This will be referred to as the single interface case.

The phase aberrations of the field at the diffraction focus position are determined by illuminating the entrance pupil with a plane wave, taking into account all effects due to propagating and evanescent waves, polarization effects and multiple reflections inside a multi-layer structure of flat layers. These are compared to the wave-front aberrations calculated using the geometrical theory presented in the appendix. Next, prior to the spot calculations, the geometrical aberrations were corrected by adjusting the phase profile of the field in the entrance pupil.

3.2. Results

We optimized a four-layer stack with thin spacer layers such that the ghost foci are kept away from the data layers other than the data layer on which is being focused. This was achieved for focusing on any of the four data layers by tuning the individual spacer layer thicknesses. The optimized four-layer stack consists of three spacer layers of unequal thickness. We have chosen a 2 μm cover-layer thickness to keep the total stack thickness as thin as possible. This 2 μm is smaller than the 3 μm used in our current experiments, but we believe that it will still give sufficient protection of the data.

In Fig. 3 a (clipped) grayscale plot is shown of the absolute values of the electric field $|\mathbf{E}|=(|E_x|^2+|E_y|^2+|E_z|^2)^{1/2}$ inside the optimized stack. The phase of this field is corrected using the results from the geometrical theory. The insets show enlarged sections of the field around the diffraction focus at L1 and around the optical axis near the L3 layer since there a ghost focus is to be expected. In accordance with the appendix the z=0 plane holds the undisturbed focus. The white line in Fig. 3 shows the irradiance $I=|\mathbf{E}|^2$ as a function of the z-coordinate. The cross-section was made through the xz-plane, yet due to the circular polarization, the (time averaged) irradiance is rotationally symmetric around the optical z-axis.

In the plot the cone of light is clearly recognizable around the focus near the point where the optical axis intersects the L1 layer. The waviness of the field around this point is due to the interference between multiple reflections. Also in the substrate the field has some structure despite the fact that there are only forward propagating waves in that region. This is explained by the fact that in the forward propagating direction there are waves that have passed through the stack at once and others that first encountered at least two reflections: these will interfere as well and thereby account for the structure observed in the substrate. Near z=6280 nm and z=6940 nm two 'ghost' foci are found which are both well separated from the L3 layer, which can be seen in the upper inset. The maximum irradiance near L3 is a factor 8.1 smaller compared to the maximum near L1.

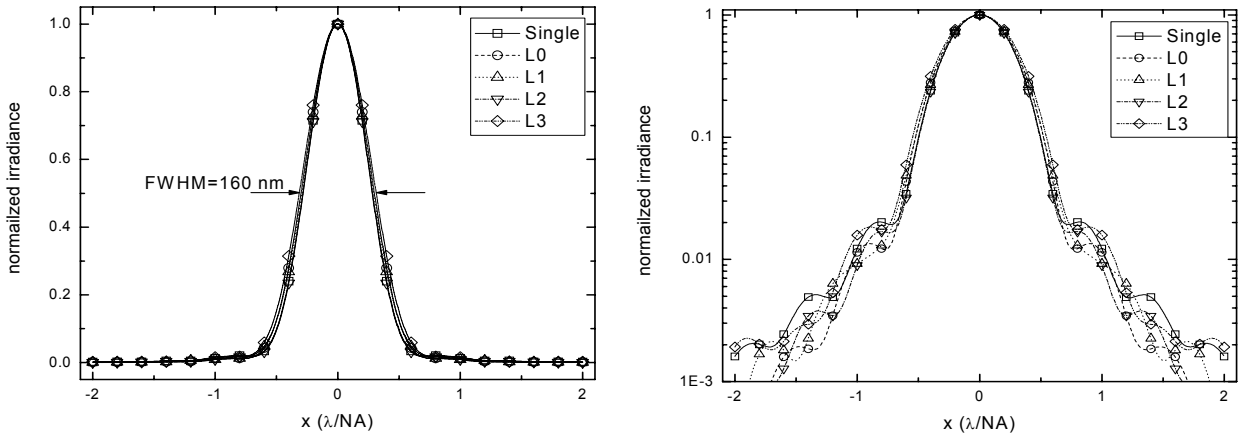

Fig. 4. Spot profiles when focusing on the layers L0-L3 compared to the spot profile for the single layer case (no data layers, no air gap). Plotted on a linear scale on the left and on a logarithmic scale on the right. For all spots the phase aberrations (defocus and spherical and higher order spherical, up to the 10th order) were corrected using the theory presented in the appendix.

Despite the rather strong interference effects due to the multiple reflections, the spot shape at focus deviates only slightly from the spot shape that is found for the single interface case. This becomes evident in Fig. 4 where the irradiance as a function of the *x*-coordinate is shown when focusing on the layers L0-L3. Compared to the single interface case a 9.0% broadening of the full width at half maximum (FWHM) occurs. This is mainly due to the aforementioned interference effects. The side lobes are smaller compared to the single layer case, which is due to the amplitude apodization of the plane waves at high incident angles.

Compared to a scaled Blu-ray Disc spot the FWHM of the spot at the L3 layer is broadened by 16.7%. All calculations were performed using a uniform pupil filling. But, in reality the pupil will be filled with a truncated Gaussian distribution. For a Blu-ray Disc system the lower rim-intensities will yield a broadening of the spot. For a Near-Field system the relatively large contribution of the *z*-component to the total electric field vector will broaden the spot. Using a truncated Gaussian distribution will lower the contribution of the *z*-component to the total field. So, the spot may in fact become somewhat smaller compared to the uniform case. The best case, i.e. taking only the in-plane components of the electric field into account gives a broadening of 8.5% when comparing the spot on L3 to a scaled Blu-ray Disc. Also increasing the refractive index of the cover- and spacer-layer material will reduce the contribution of the *z*-component of the field and thereby reduce the spot width.

From the field inside the stack the phase aberrations are calculated in terms of Zernike polynomials. The resulting Zernike coefficients found when focusing on L1 are shown in Table 1. For comparison the coefficients were also calculated and given for the single layer case while focusing at a depth of 6.8 μm using the formalism given in the appendix. It is worth noting that for a high NA system, the defocus coefficient is not equal to zero in the diffraction focus at the position where the aberrations are minimum. Apart from the defocus coefficient the results in Table 1 are in close agreement. The reason for this is that the phase of the field in the multi-layer stack varies very rapidly over the pupil plane, which means that the lower aberration terms will not deviate much as these follow only the smoothly varying phase. It is in the very high orders that differences are found between the two approaches.

Table 1. Calculated Zernike coefficients

Zernike coefficient		complete stack	single layer case
Defocus	A_{20} ($m\lambda_{rms}$)	-4.9	21.2
Spherical	A_{40} ($m\lambda_{rms}$)	-250.6	-242.7
Higher Order Spherical	A_{60} ($m\lambda_{rms}$)	-98.0	-95.9
	A_{80} ($m\lambda_{rms}$)	-37.4	-36.0
	A_{100} ($m\lambda_{rms}$)	-14.8	-13.7

4. OPTICAL PATH DESIGN

For the example in Fig. 1, a focus jump from the deepest L0-layer to the upper L3-layer requires a change in spherical aberration of 257 $m\lambda_{rms}$. This holds only when the undisturbed focus is adjusted to the position were the aberrations are minimized. In far field systems like BD the lens-to-disc distance can be changed to adjust the focus. For the NF system the air-gap rather than the focus position is controlled by actuating the lens. So this degree of freedom is lost. Here an active liquid crystal (LC) compensation device as proposed in earlier work[11] is used to correct for defocus, spherical aberration and the higher order spherical aberration terms.

4.1. Objective lens design

Using Zemax™, first an *NA*=1.6 glass molded double aspherical objective lens was designed using a N-LaSF31 SIL for a t_{cover}=2 μm thick cover-layer with a refractive index of 1.7, see Fig. 5. The objective lens has a pupil diameter of 2.5 mm. The SIL has a radius of R_{SIL}=0.5 mm. The tolerances for total wave-front aberrations W_{tot}=15 $m\lambda_{rms}$ of this design are listed in Table 2. The tightest tolerance of the current design is on the decenter of the aspheres.

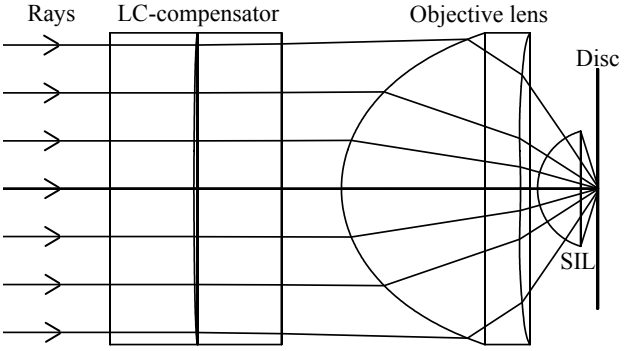

Fig. 5. Lay-out of the objective lens design with a N-LaSF31 SIL and 2 μm cover with n=1.7 and LC-compensation device for switching between the four data layers.

Table 2. Objective lens design W_{tot}=15 mλ_{rms} tolerances.

Field	0.45	°
SIL thickness	22	μm
SIL decenter	9	μm
Asphere decenter	0.4	μm

4.2. LC-compensator

Together with the objective lens design, a LC-compensator was designed for changing the focus position between the different data layers with the spacer layers according to the stack design example given in the former section. The liquid crystal cell was constructed from two 0.7 mm thick SF11 glass plates of which the left plate, in Fig. 5, has an aspherical surface that is in contact with the liquid crystal material. The liquid crystal material has an extraordinary refractive index n_e matched to the SF11 glass and a birefringence Δn=0.4.[12] Switching between the layers is done by changing the effective refractive index of the LC material, n_{LC}. The lens aperture was decreased compared to the objective lens to keep the numerical aperture at the L0-layer at the desired NA=1.6. The results for all four layers are shown in Table 3. At the exit surface of the SIL a 50 μm spot size is found when focusing through the entire stack. This leaves a ±10 μm centering tolerance when using a 70 μm diameter SIL-tip.

Table 3. Numerical aperture and total wave front at the different layers.

layer	n_{LC}	NA	W_{tot} (mλ_{RMS})
L0	1.84	1.60	22.4
L1	1.74	1.58	16.7
L2	1.64	1.56	22.6
L3	1.54	1.54	2.4

The light incident on the LC-compensator needs to be linearly polarized which means that after the LC-compensator a quarter-wave plate is needed to make the light circularly polarized. This can be integrated into the LC-compensator itself by making the second substrate into a quarter wave plate.

CONCLUSIONS

Applying phase corrections to the field in the entrance pupil yields diffraction-limited spots at the required data layers. This despite the strong interference effects due to multiple reflections between the quite thin layers. Some broadening of the spots is found in the simulations that is mainly due to the contribution of the z-component of the field. A truncated Gaussian irradiance distribution in the entrance pupil will bring this contribution down. Also a higher refractive index for the cover- and spacer-layers may further reduce this contribution and thereby reduce the spot width.

We have shown that a four-layer stack with thin spacer layers can be optimized such that the ghost foci are kept away from the data layers other than the data layer on which is being focused. This was achieved for focusing on any of the four data layers by tuning the individual spacer layer thicknesses. The optimized four-layer stack consists of three spacer layers of unequal thickness.

The amount of spherical aberration correction needed when changing focus from the L0 to the L3 layer is comparable to what is found when jumping between layers in a Blu-ray disc four-layer system. An objective lens and LC-compensator were designed that enable reading and writing from all four layers.

This study has taken away concerns we had on how the interference between the multiple reflections affects the spot shape. The results justify the aforementioned roadmap to a 500 GB four-layer cover-incident NF system and experimental work on such a system.

Appendix: Aberration coefficients for focusing in a cover-layer with arbitrary numerical aperture

In this appendix we derive exact expressions for the Zernike coefficients associated with an expansion of the wave front aberration caused by focusing a spherical wave from one medium into a second medium. In our case the first medium is the SIL and the second medium the cover-layer. The derivation is exact for arbitrarily high NA and follows a recently published formalism[9] with which the wave front aberrations are studied that are caused by focusing through a parallel plate with the diffraction focus behind the plate shifted by some distance with respect to the undisturbed focus. The current derivation describes the wave front aberrations and focal shift with just a single transition between two media with the diffraction focus and the focal shift in the second medium. We will show that the expressions for the Zernike coefficients for the case of a single transition are identical to those in the case of a parallel plate. Evidently, the focal shift for the single transition case is not identical to that of the parallel plate case with the focus behind the plate. The choice of the position of the undisturbed focus is important when calculating the aberration corrections required for a perfectly corrected diffraction focus at a given depth in the second medium.

Consider a propagating spherical wave, virtually focused at point O at $z=0$, see Fig. A.1. The exit pupil of the focusing system is situated in a first medium with refractive index n_1 that is real. At $z=-d_1$ the beam is transmitted through an abrupt transition to a semi-infinite second medium with refractive index n_2 that is also real which leads to a focal shift d_f. In the first medium we have a general ray with propagation vector $\boldsymbol{k}_1$ and in the second medium the ray has propagation vector $\boldsymbol{k}_2$ both of which we assume to be real. We define the wave-front aberration function W for a single transition with reference to a point O' as the difference in optical path for a general ray along OP_1P_2' and the optical path for the chief ray along OAO'.

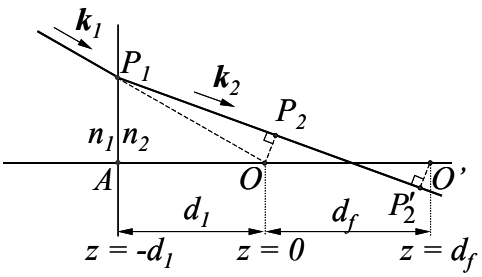

Fig. A.1. Chief ray and general ray of a beam that is virtually focused in point O at z=0 and that is refracted at a single transition between refractive index n_1 and n_2 at z=-d_1. The incident beam is normal to the transition. The aberration function is taken with reference to a point O'.

$$W_{O'} = [OP_1P_2'] - [OAO'] \,. \tag{A.1}$$

The phase aberration is $k_0 = 2\pi/\lambda_0$ times the aberration function $W_{O'}$. We express the phase due to the respective parts of the optical path as an inner product of the propagation vector and the (difference of) position vectors $\boldsymbol{r}$:

$$\begin{aligned} k_0 W_{O'} = &\left(\boldsymbol{k}_1 \cdot \boldsymbol{r}_{P_1} + \boldsymbol{k}_2 \cdot (\boldsymbol{r}_{P_2} - \boldsymbol{r}_{P_1}) + \boldsymbol{k}_2 \cdot (\boldsymbol{r}_{P'_2} - \boldsymbol{r}_{P_2})\right) \\ &- \left(\boldsymbol{k}_1 \cdot \boldsymbol{r}_A + \boldsymbol{k}_2 \cdot (\boldsymbol{r}_O - \boldsymbol{r}_A) + \boldsymbol{k}_2 \cdot (\boldsymbol{r}_{O'} - \boldsymbol{r}_O)\right) \,. \end{aligned} \tag{A.2}$$

We thus find for the aberration function with reference to point O' for a single transition:

$$k_0 W_{O'} = \left(k_{z2} - k_{z1}\right) d_1 + k_{z2} d_f \,, \tag{A.3}$$

where we omitted an irrelevant constant phase term $-d_1\left(k_2 - k_1\right) - k_2 d_f$ and in which $k_{zi} = \sqrt{k_i^2 - k_r^2}$. It is now convenient to write the aberration function in the form

$$W_{O'} = d(F_2 + \alpha F_1) \,, \tag{A.4}$$

where $d = d_1 + d_f$ and $\alpha = -d_1 / d$ and using the functions $F_i = k_{zi} / k_0$ for i =1, 2. The optimal focal shift d_f for the best diffraction focus is determined by the position at which the wave-front variance is minimum. The optimal focal shift d_f can be found by minimization of the variance $W_{O'rms}^2 = \langle W_{O'}^2 \rangle - \langle W_{O'} \rangle^2$ in α. This minimum was found for:

$$\alpha = -\frac{\langle F_1 F_2 \rangle - \langle F_1 \rangle \langle F_2 \rangle}{\langle F_1^2 \rangle - \langle F_1 \rangle^2} , \tag{A.5}$$

with the averages over the exit pupil:

$$\begin{aligned} \langle F_i \rangle &= \frac{2}{3NA^2}\left[n_i^3 - \left(n_i^2 - NA^2 \right)^{3/2} \right] \quad \text{and} \quad \langle F_i^2 \rangle = n_i^2 - \tfrac{1}{2} NA^2 \\ \langle F_1 F_2 \rangle &= \frac{1}{4NA^2}\left[n_1 n_2 \left(n_1^2 + n_2^2 \right) - \left(n_1^2 + n_2^2 - 2NA^2 \right) \times \sqrt{n_1^2 - NA^2}\sqrt{n_2^2 - NA^2} \right. \\ &\quad \left. + \left(n_1^2 - n_2^2 \right)^2 \ln\left(\frac{\sqrt{n_1^2 - NA^2} + \sqrt{n_2^2 - NA^2}}{n_1 + n_2} \right) \right] . \end{aligned} \tag{A.6}$$

Exact analytical expressions can be found for the Zernike coefficients of the expansion of the aberration function (A.3) in Zernike polynomials of radial order n and azimuthal order 0:

$$A_n^0 = \frac{n+1}{\pi} \int_0^{2\pi} \int_0^1 W(\rho) Z_n^0(\rho) \rho d\rho d\theta = d n_2 \xi_n \left(\frac{NA}{n_2} \right) + \alpha d n_1 \xi_n \left(\frac{NA}{n_1} \right) , \tag{A.7}$$

with the functions

$$\xi_n(\varepsilon) = 2(n+1) \int_0^1 \sqrt{1 - \varepsilon^2 \rho^2}\, P_{\frac{n}{2}}(2\rho^2 - 1) \rho d\rho , \tag{A.8}$$

in which $\rho = k_r / \left(NA\, k_0 \right)$ is the normalized radial coordinate and $P_{\frac{n}{2}}(2\rho^2 - 1)$ are the Legendre polynomials of order $n/2$ and argument $(2\rho^2 - 1)$. The coefficients found with (A.7) can be expressed in units of wavelength by division with λ_0 and may be multiplied with the well-known RMS normalization factor $\sqrt{1/(n+1)}$ to obtain the RMS coefficients. We found solutions for $\xi_n(\varepsilon)$ that differ by a factor $n+1$ from the solutions reported before[9]:

$$\begin{aligned} \xi_2(\varepsilon) &= \frac{8 - 10\varepsilon^2 - (8 - 6\varepsilon^2 - 2\varepsilon^4)\sqrt{1 - \varepsilon^2}}{5\varepsilon^4} \\ \xi_4(\varepsilon) &= \frac{96 - 168\varepsilon^2 + 70\varepsilon^4 - (96 - 120\varepsilon^2 + 22\varepsilon^4 + 2\varepsilon^6)\sqrt{1 - \varepsilon^2}}{21\varepsilon^6} \\ \xi_6(\varepsilon) &= \frac{640 - 1440\varepsilon^2 + 1008\varepsilon^4 - 210\varepsilon^6}{45\varepsilon^8} \\ &\quad - \frac{(640 - 1120\varepsilon^2 + 528\varepsilon^4 - 46\varepsilon^6 - 2\varepsilon^8)\sqrt{1 - \varepsilon^2}}{45\varepsilon^8} \\ \xi_8(\varepsilon) &= \frac{3584 - 9856\varepsilon^2 + 9504\varepsilon^4 - 3696\varepsilon^6 + 462\varepsilon^8}{77\varepsilon^{10}} \\ &\quad - \frac{(3584 - 8064\varepsilon^2 + 5920\varepsilon^4 - 1520\varepsilon^6 + 78\varepsilon^8 + 2\varepsilon^{10})\sqrt{1 - \varepsilon^2}}{77\varepsilon^{10}} \\ \xi_{10}(\varepsilon) &= \frac{18432 - 59904\varepsilon^2 + 73216\varepsilon^4 - 41184\varepsilon^6 + 10296\varepsilon^8 - 858\varepsilon^{10}}{117\varepsilon^{12}} \\ &\quad - \frac{(18432 - 50688\varepsilon^2 + 50176\varepsilon^4 - 21280\varepsilon^6 + 3480\varepsilon^8 - 118\varepsilon^{10} - 2\varepsilon^{12})\sqrt{1 - \varepsilon^2}}{117\varepsilon^{12}} . \end{aligned} \tag{A.9}$$

REFERENCES

1. F. Zijp et al, "Near-field Read-out of a 50-GB First-surface Disc with NA=1.9 and a Proposal for a Cover-layer incident Dual-layer Near-field System", *Proc. SPIE* **5380** pp.209-223, 2004.
2. M. Shinoda et al, "High-density Near-field Optical Disc recording using Phase Change Media and Polycarbonate Substrate", *Proc. SPIE* **5380** pp.224-232, 2004.
3. C.A. Verschuren, F. Zijp, J.I. Lee, J.M.A. van den Eerenbeemd, D.M. Bruls, "Cover-layer incident Near-Field Recording: Towards 4-layer Discs using Dynamic Tilt Control", *Tech. Digest of ODS*, 2006, paper TuB1; also published in these proceedings.
4. D.M. Bruls et al, "High Data Transfer Rate Near-Field Recording System with a Solid Immersion Lens for Polymer Cover–Layer Discs", *Tech. Digest of ODS*, 2006, paper MC 4; also published in these proceedings.
5. A. Padiy, B. Yin, C.A. Verschuren, J.I. Lee, R. Vlutters and Th. Jansen, "Signal processing for 35GB on a single-layer Blu-ray Disc", *Proc. SPIE*, **5380** pp. 56-70, 2004
6. F. Zijp, J.M.A. van den Eerenbeemd, H.P. Urbach, C.A. Verschuren, "Effects of Polarization on Wave Front Measurements and Manufacturing of Solid Immersion Lenses for Near-Field Optical Recording", *Jpn. J. Appl. Phys.* **45 2b** 1341-1347, 2006.
7. B. Richards, E. Wolf, "Electromagnetic Diffraction in Optical Systems II. Structure of the Image Field in an Aplanatic System", *Proc. Roy. Soc. A* **253**, pp.358-379, 1959.
8. A.S. van de Nes, L. Billy, S.F. Pereira and J.J.M. Braat, "Calculation of the Vectorial Field Distribution in a Stratified Focal Region of a High Numerical Aperture Imaging System", *Opt. Exp.* **12** pp.1281-1293, 2004.
9. S. Stallinga, "Compact Description of Substrate Related Aberrations in High NA Optical Disc Read-out", *Appl. Opt.* **44**, pp.849-858, 2005.
10. K. Mishima, H. Inoue, M. Aoshima, T. Komaki, H. Hirata and H. Ustunomiya, "Inorganic Write-Once Disc with Quadruple Recording Layers for Blu-ray Disc System", *Proc. SPIE* **5069,** pp. 90-97, 2003
11. S. Stallinga, J. Vrehen, J. Wals, H. Stapert and E. Verstegen, "Liquid crystal aberration compensation devices", *Optical Storage and Optical Information Processing, Proceedings of SPIE* **4801**, pp. 50-59, 2000.
12. S Gauza, C.H. Wen, B Tan and S.T. Wu, "UV Stable High Birefringence Liquid Crystals", *Jpn. J. Appl. Phys.* **43**, pp 7176–7180, 2004.